ansa-Metallocene derivatives [1]
XLI. Chiral ansa-Magnesocene complexes–syntheses, crystal structures and structural dynamics in solution

Hans-Robert H. Damrau, Armin Geyer, Marc-Heinrich Prosenc, Armin Weeber,
Frank Schaper, Hans-Herbert Brintzinger [*]

Fakultät für Chemie, Universität Konstanz, D-78434 Konstanz, Germany

Abstract

A series of chiral ansa-magnesocene complexes with dimethylsilanediyl- or ethanediyl-bridged, substituted cyclopentadienyl or indenyl ligands, prepared in form of their THF adducts, has been structurally characterized by diffractometric crystal structure determination and by NMR studies in solution. The hapticities of the ring ligands vary between η^1 and η^5, depending on the nature of the interanular bridge and the C_5 ring substituents. A racemic configuration is preferred by Mg bis-indenyl complexes with either Me_2Si- or C_2H_4-bridges in the solid state and in solution, while meso isomers predominate for *t*-butyl-substituted ansa-magnesocenes. © 1998 Elsevier Science S.A.

Keywords: Magnesium; ansa-Metallocene; Chiral; Configuration; Hapticity

1. Introduction

Whereas numerous chiral ansa-metallocene complexes have been obtained in recent years for metals of group 4 and 3, no representative for this class of compounds with a group 2 central metal has been described so far. Unbridged metallocenes of the heavier group 2 metals have been reported to have a bent geometry [2–7], which is inherently suitable for the introduction of a bridging unit. C_2H_4- or Me_2Si-bridged calcocene and barocene derivatives with stabilizing THF ligands have indeed recently been obtained and structurally characterized [8–10].

Even though essentially linear geometries with parallel, η^5-coordinated ring ligands are found for magnesocene complexes such as $(C_5H_5)_2Mg$, $(C_5H_4^tBu)_2Mg$ and $(C_5(CH_3)_5)_2Mg$ [11–13], Burger has recently obtained Me_2Si-, Me_2C- and Me_4C_2-bridged biscyclopentadienyl Mg complexes, with a bent geometry stabilized by neutral supporting ligands [14]. From the crystal structures reported for these group 2 metallocene com-

plexes it is apparent that their C_5 ring ligands are frequently coordinated to the metal center with reduced hapticity [10,14]. In order to clarify how these structural features affect the relative stabilities and interconversion kinetics of the meso and racemo diastereomers expected for chiral ansa-metallocene derivatives of this type, we have synthesized ring-bridged magnesocene complexes, which are chiral due to an appropriate substitution of their C_5-ring ligands. In the following, we report on the hapticity patterns of these complexes and on their structural dynamics in solution.

2. Results and discussion

2.1. Syntheses and crystal structures

ansa-Magnesocene complexes containing substituted cyclopentadienyl or indenyl ligands, connected by ethanediyl or silanediyl bridges, were prepared by reaction of the corresponding neutral ligand molecules with one equivalent of dibutyl magnesium in refluxing heptane [15–17]. Addition of THF yields, from sufficiently concentrated solutions (sometimes after covering with a

---

[*] Corresponding author.
[1] For part XL, see Ref. [1].

hexane layer), the respective THF adducts in form of off-white powders or, in some instances, of colorless crystals (see Section 4).

Crystallographic structure determinations of these compounds proved unexpectedly difficult, mainly because of frequent positional disordering, which appears to be an inherent property of these compounds. Nevertheless, the topologies of a series of chiral ansa-magnesocene complexes could be reliably established. In analysing the resulting structural data, we have adopted a Mg–C distance of 275 pm as the limit of a bonding interaction. This limit appears to provide a reasonably clear-cut distinction between bonding and nonbonding Mg–C interactions; only in a few instances do ambiguities arise from Mg–C distances close to this limit. The number X of adjacent Mg–C bonds for each ligand unit is then considered to define its hapticity η^X; its point of attachment to the Mg center will be represented in the following figures by the centroid Z of the respective C_X segment.

The C_2H_4-bridged bis-indenyl complex **1**, $C_2H_4(\text{ind})_2\text{Mg(THF)}_2$ gave, from THF–hexane solutions, crystals suitable for an X-ray diffraction study. Their unit cell contains two crystallographically independent molecules (Fig. 1, Table 1). In both of these, the overall geometry is that of the racemic (rather than of the meso) isomer. Mg–C bond distances vary rather strongly: In each case, one Mg–C distance is short (231–240 pm) while the two adjacent Mg–C bonds are longer and differ more widely (245–275 pm); the remaining two Mg–C distances (278–316 pm) are even

longer and, in general, beyond the range considered as bonding.

In molecule **1**(1), one of the indenyl rings is coordinated via the three C atoms which are not part of the C_6-ring, as is normally found in η^3-bound indenyl complexes [18], while the second ring has the Mg atom closest to the bridge-head C atom and its two neighbours on either side, including one of the C atoms in angular position. In molecule **1**(2), which is practically C_2-symmetric, both indenyl rings are bound in the normal allylic η^3 manner to the Mg atom.

As observed by Burger [14] for unsubstituted ansa-magnesocene complexes, the bent geometry induced by the C_2H_4 bridge requires that the ensuing coordination gap is filled by supporting ligands. In both molecules of complex **1**, two THF ligands are coordinated to the Mg center in the mid-plane of the molecule. These extra ligands appear to reduce the hapticity of both C_5-ring ligands to a bis-η^3-type coordination, due to electronic and/or steric repulsion between the THF ligands and the indenyl rings. The geometries of molecules **1**(1) and **1**(2) demonstrate that binding via the allylic and via the bridgehead-centered C_3 segments of the indenyl ligands are of comparable stability for this ethanediyl-bridged bis-indenyl complex.

To study the effects of a shorter Me_2Si bridge on Mg-indenyl binding modes, we tried to prepare the otherwise analogous complex $\text{Me}_2\text{Si(ind)}_2\text{Mg(THF)}_2$. For this complex, however, we could not obtain crystals suitable for an X-ray study. An alkyl-substitued complex of this type, $\text{Me}_2\text{Si}(2\text{-methyl-}6,7,8,9\text{-tetrahydro-}$
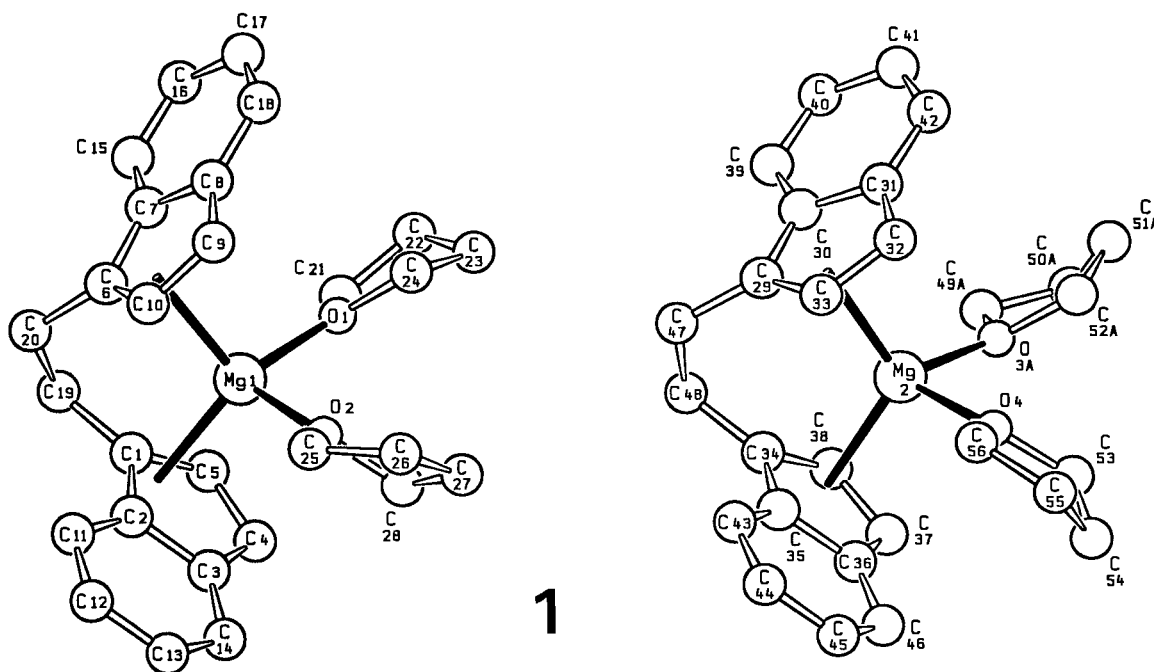

Fig. 1. Structure of complex **1** (left: molecule **1**(1), right: molecule **1**(2)). For atoms with positional disorder only one set is shown (labelled with suffix A). Hydrogen atoms omitted for clarity.

Table 1
Selected distances[a] (pm) and angles (deg) for complexes **1–4**

1(1)		1(2)		2(1)		2(2)		3		4	
Mg(1)–O(1)	198.9(2)	Mg(2)–O(3A)	206.5(5)	Mg(1)–O(1)	202.3(4)	Mg(2)–O(3)	200.4(4)	Mg(1)–O(1)	203.6(7)	Mg(1)–O(1)	202.1(7)
Mg(1)–O(2)	200.5(2)	Mg(2)–O(4)	202.3(6)	Mg(1)–O(2)	199.9(4)	Mg(2)–O(4)	201.6(5)			Mg(1)–O(2)	202.2(8)
Mg(1)–C(1)	232.8(3)	Mg(2)–C(29)	263.3(3)	Mg(1)–C(4)	240.8(7)	Mg(2)–C(42)	232.5(6)	Mg(1)–C(1)	242.3 (12)	Mg(1)–C(1)	233.8(10)
Mg(1)–C(2)	268.2(3)	Mg(2)–C(32)	257.8(3)	Mg(1)–C(5)	242.0(6)	Mg(2)–C(43)	240.2(6)	Mg(1)–C(2)	252.5 (12)	Mg(1)–C(2)	247.4(10)
Mg(1)–C(5)	245.1(3)	Mg(2)–C(33)	232.3(3)	Mg(1)–C(6)	263.5(7)	Mg(2)–C(44)	271.4(6)	Mg(1)–C(3)	258.7(10)	Mg(1)–C(3)	268.3(10)
Mg(1)–C(6)	251.2(3)	Mg(2)–C(34)	247.8(3)	Mg(1)–C(18)	228.7(7)	Mg(2)–C(56)	234.3(6)	Mg(1)–C(4)	247.8(11)	Mg(1)–C(4)	263.6(11)
Mg(1)–C(9)	275.2(3)	Mg(2)–C(35)	278.1(3)	Mg(1)–C(19)	241.9(6)	Mg(2)–C(57)	241.3(6)	Mg(1)–C(5)	236.5 (12)	Mg(1)–C(5)	240.7(10)
Mg(1)–C(10)	231.4(3)	Mg(2)–C(37)	269.2(3)	Mg(1)–C(20)	278.6(7)	Mg(2)–C(58)	271.8(6)	Mg(1)–C(6)	238.9 (10)	Mg(1)–C(6)	275.4(10)
		Mg(2)–C(38)	240.6(3)					Mg(1)–C(7)	240.2 (10)	Mg(1)–C(10)	234.7(9)
								Mg(1)–C(8)	242.4 (12)		
								Mg(1)–C(9)	242.9 (10)		
								Mg(1)–C(10)	234.2 (11)		
				Si(1)–C(4)	185.3(7)	Si(2)–C(56)	186.7(6)			Si(1)–C(1)	187.1(11)
				Si(1)–C(18)	184.8(7)	Si(2)–C(42)	185.2(6)			Si(1)–C(6)	184.2(9)
				C(18)–Si(1)–C(4)	105.1(3)	C(42)–Si(2)–C(56)	104.9(3)			C(1)–Si(1)–C(6)	104.1(4)
				Z(1)–C(4)–Si(1)[c]	191	Z(3)–C(42)–Si(2)[c]	192	Z(1)–Mg(1)–Z(2)[c]	130.4	Z(1)–C(1)–Si(1)[c]	167
				Z(2)–C(18)–Si(1)[c]	193	Z(4)–C(56)–Si(2)[c]	190			Z(2)–C(6)–Si(1)[c]	178
O(1)–Mg(1)–O(2)	91.62(8)	O(3A)–Mg(2)–O(4)	94.40(1)	O(1)–Mg(1)–O(2)	88.4(2)	O(3)–Mg(2)–O(4)	87.1(2)			O(1)–Mg(1)–O(2)	91.5(3)
X(1)–Mg(1)–X(2)[b]	112.7	X(3)–Mg(2)–X(4)[b]	122.0	X(1)–Mg(1)–X(2)[b]	115.0	X(3)–Mg(2)–X(4)[b]	116.0			Z(1)–Mg(1)–C(10)[c]	116.7
Cp(1)–Cp(2)[d]	74	Cp(3)–Cp(4)[d]	65	Cp(1)–Cp(2)[d]	70	Cp(3)–Cp(4)[d]	70	Cp(1)–Cp(2)[d]	63	Cp(1)–Cp(2)[d]	77

[a] Only Mg–C distances < 280 pm are listed.
[b] X(1), X(2): centroids of lower- and higher-numbered C_X-segment, respectively.
[c] Z(1), Z(2): centroids of lower- and higher-numbered C_5-ring, respectively.
[d] Cp(1), Cp(2): mean planes of lower- and higher-numbered C_5-ring, respectively.

benz[e]indenyl)$_2$-Mg(THF)$_2$ (Me$_2$Si(2-Methbzind)$_2$Mg(THF)$_2$, **2**), gave suitable crystals, however. The diffractometric structure determination yielded again a unit cell which contains two crystallographically independent molecules, one of which shows some disorder in the hydrogenated six-ring, and one molecule of heptane for two magnesocene molecules. For both complex molecules, we find a racemic geometry, which is close to C$_2$ symmetry, especially for molecule **2**(2) (Fig. 2, Table 1).

The Mg-indenyl binding, however, differs substantially from that in complex **1**: the Mg atom is now bound in an exocyclic η^3 geometry: it is closest to a C$_3$ segment comprising the bridgehead and the adjacent angular position as well as the neighboring C atom in the aromatic six-ring. This geometry appears to be virtually tension-free with regard to the Me$_2$Si bridge as indicated by close-to-tetrahedral C(ipso)–Si–C(ipso) angles of 105° and a deviation of the C(ipso)–Si bonds from the adjacent C$_5$-ring mean planes to the outside of the complex molecule by 11–13°. Related exocyclic η^3-coordination geometries have previously been reported for some metallocenes which would otherwise be severely strained by a short single-atom bridge [19–22].

To characterize also chiral ansa-magnesocenes with cyclopentadienyl ligands, we prepared the tetramethylethanediyl-bridged, *t*-butyl substituted complex Me$_4$C$_2$(3-^{t}Bu-C$_5$H$_3$)$_2$Mg(THF) (**3**). From concentrated heptane–THF solutions we obtained colorless plates of complex **3**. The X-ray diffraction analysis of these crystals was encumbered by a disordered orientation of the C$_2$ bridge, which adopts, with equal probability, a λ and a δ conformation [23]. This disorder renders the structural data for this complex of marginal quality. Nevertheless, there are no doubts about the following structural features (Fig. 3, Table 1): The complex is present as its meso diastereomer, with both 3-*t*-butyl groups on the same side of the C(ipso)–Si–C(ipso) plane; both C$_5$ ring ligands are η^5-coordinated to the Mg center, with Mg–C distances of ca. 230–260 pm. Due to its meso configuration, one coordination site of complex **3** is shielded by the two *t*-butyl groups; at the more open site, one THF molecule is coordinated to the Mg center. The coordination of only one THF ligand as well as the presence of cyclopentadienyl rather than indenyl ligands might both contribute to the preference for a bis-η^5-coordination in this ethano-bridged complex molecule.

The Me$_2$Si-bridged, *t*-butyl-substituted complex Me$_2$Si(3-^{t}Bu-C$_5$H$_3$)$_2$Mg(THF)$_2$ (**4**), finally, was obtained in crystalline form from concentrated THF–heptane solution. The diffractometric structure determi-
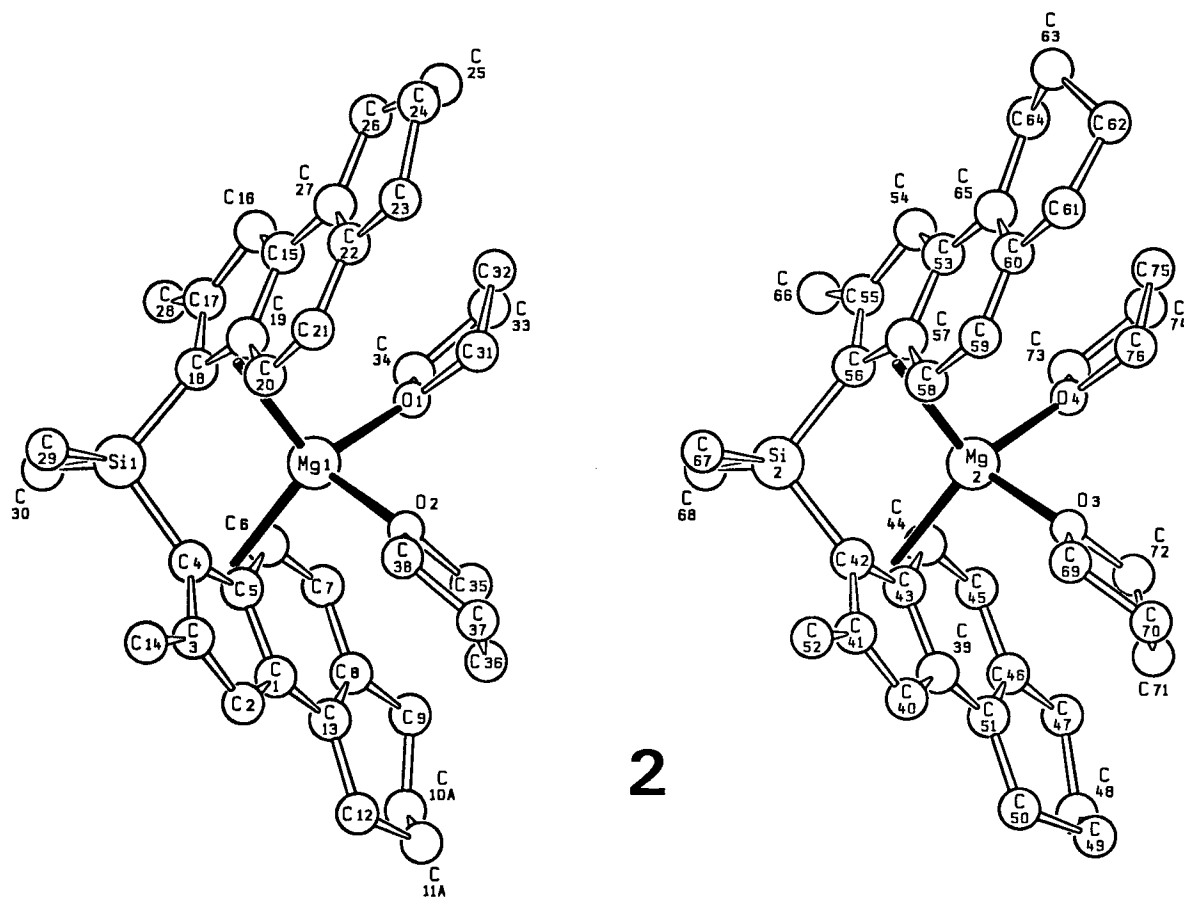

Fig. 2. Structure of complex **2** (left: molecule **2**(1), right: molecule **2**(2)). Other features as in Fig. 1.
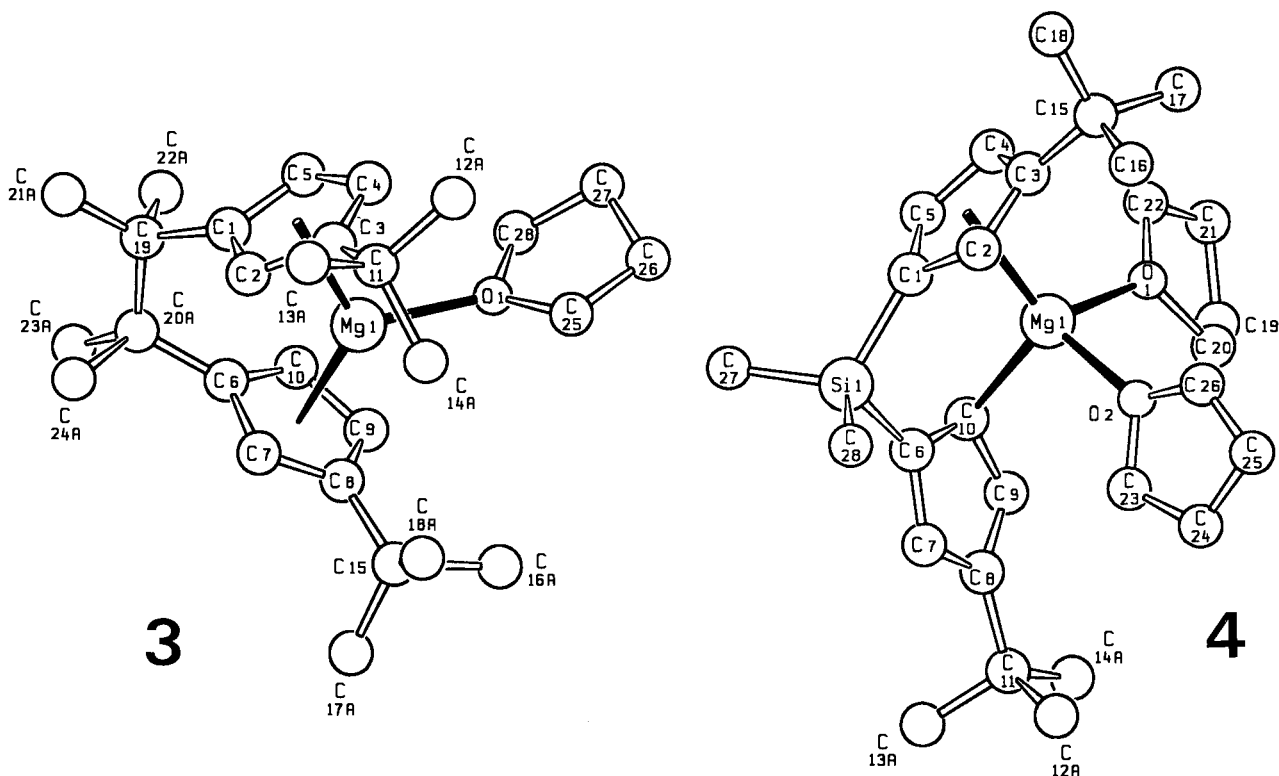
Fig. 3. Structures of complexes **3** (left) and **4** (right). Other features as in Fig. 1.

nation, while of marginal quality again, shows the following connectivities (Fig. 3 and Table 1): one C_5 ring is coordinated to the Mg center with a hapticity approaching η^5, with three short (234–241 pm) and two longer Mg–C distances (264–268 pm). The other C_5 ring is bound in a η^1-manner, with only one short Mg–C distance of 236 pm, all other Mg distances being longer than 270 pm. The η^1-coordination of one of the C_5 rings allows for a large dihedral angle of 77° between the mean planes of both C_5 rings. This affords again an essentially tension-free geometry at the Me_2Si bridge: While the Si–C(ipso) bond adjacent to the η^5-coordinated C_5 ring deviates by 13° from the C_5-ring mean plane, the other one deviates by only 2° from that of the η^1-coordinated C_5 ring. The C(ipso)–Si–C(ipso) angle (104°) is again much closer to tetrahedral geometry here than in Me_2Si-bridged bis-η^5-coordinated zirconocenes, where it adopts values of ca. 95° [24].

The increased coordination gap associated with the large interplanar angle of 77° allows for coordination of two THF molecules (rather than only one as in **3**). Complex **4** adopts again a configuration with both *t*-butyl groups on the same side of the C(ipso)–Si–C(ipso) plane; it can thus be considered as a 'pre-meso' species [24], which would be transformed to the meso form upon conversion of the η^1-bound C_5 ring to an η^5-coordination.

In summarizing the structural data for complexes **1**–**4**, we find that their hapticities vary between η^5,

endo- and exocyclic η^3 and η^1, depending on the nature of the interanular bridge and the C_5 ring substituents. In complexes **1**, **2** and **4**, coordination at the Mg center approaches tetrahedral geometry: the centroids of the bonded C_X segments (with Mg–C distances ≤ 275 pm) span centroid–Mg–centroid angles of 112–122°, the THF ligands O–Mg–O angles of 87–92°. For complexes **1** and **2**, the O–Mg–O angle is approximately bisected by the centroid–Mg–centroid plane and vice versa; for complex **4**, this relationship holds for the plane containing the Mg atom, the coordinated C atom of the η^1-bound C_5 ring and the centroid of the η^5-coordinated C_5 ligand. In complex **3**, the Mg center approaches a trigonal planar geometry, with a centroid–Mg–centroid angle of 130° and a practically coplanar arrangement of the two C_5-ring centroids, the THF–O atom and the Mg center.

With regard to the configurations of the ansa-magnesocene complexes studied here, it is remarkable that both bis-indenyl complexes are found to crystallize in form of their racemo isomers while both cyclopentadienyl complexes occur in a meso-type configuration. In the case of the bis-indenyl complexes, two factors appear to contribute to the greater stability of the racemo isomers: (i) The C_6 rings attached to the α-positions of both C_5 ring ligands would incur substantial mutual repulsion in a meso isomer. (ii) The inherent tendency of the indenyl ligands to adopt a bis-η^3-coordination allows the C_6-ring part of these ligands to move away
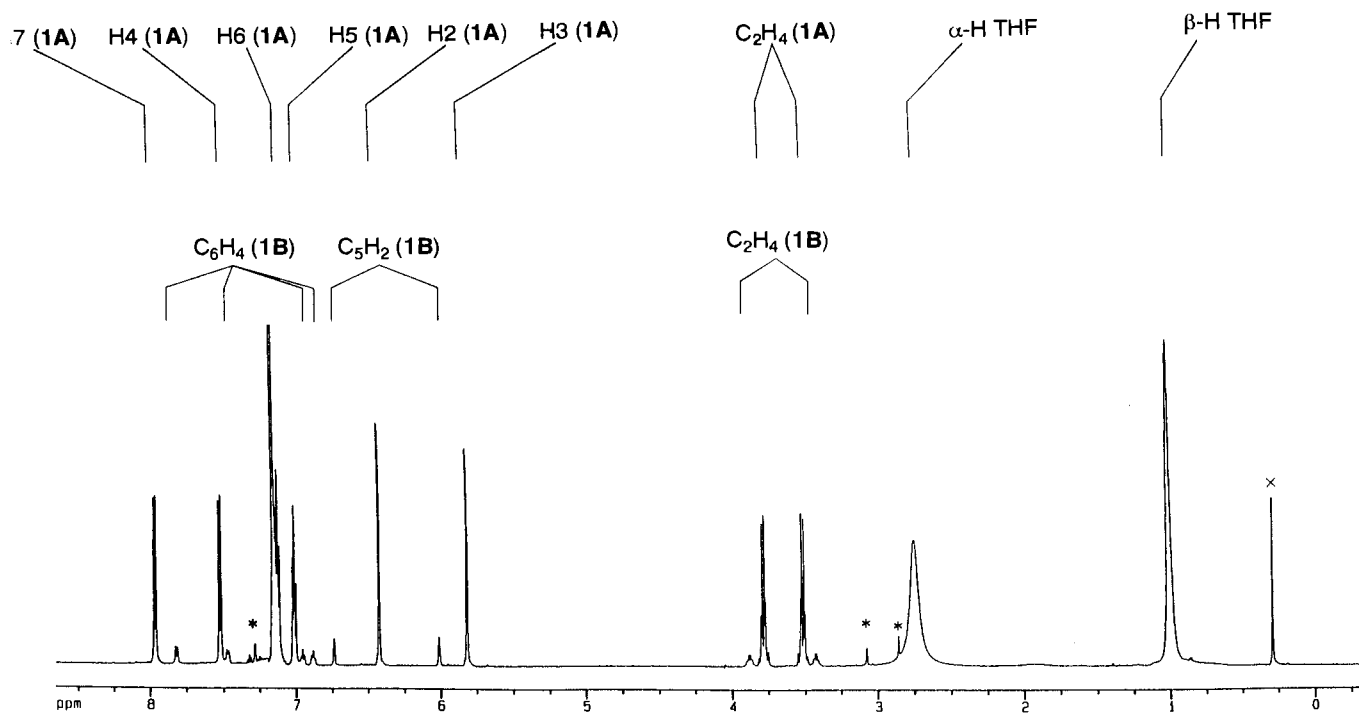
Fig. 4. ^{1}H NMR spectra of complex **1** in C_6D_6 solution (25°C, 600 MHz, extraneous signals: * hydrolysis product, + silicon grease). Assignments derived from COSY and ROESY spectra.

Table 2
^{1}H NMR shifts for complex **1** (in ppm, 25°C, 600 MHz)

1A[a]	**1B**[a]	**1A**[b]	**1B**[b]	Assignment
7.75(d)	7.59(d)	7.96(d)	7.82(d)	C_6H_4
7.36(d)		7.51(d)	7.47(d)	C_6H_4
6.86(t)	6.68(t)	7.12(t)	6.95(t)	C_6H_4
6.77(t)	6.62(t)	7.01(t)	6.93(t)	C_6H_4
6.24(d)	6.72(d)	6.42(d)	6.73(d)	C_5H_2
5.73(d)	6.02(d)	5.81(d)	6.01(d)	C_5H_2
3.22(b)	3.22(b)	2.74(b)	2.74(b)	THF
1.63(b)	1.63(b)	1.00(b)	1.00(b)	THF
3.57(m)	3.70(m)	3.78(m)	3.88(m)	H_4C_2
3.28(m)	c	3.51(m)	3.42(m)	H_4C_2

[a] In CD_2Cl_2.
[b] In C_6D_6.
[c] Presumably underneath the THF signal at 3.22 ppm.

Table 3
^{1}H NMR shifts for complex **2** (in ppm, 25°C, CD_2Cl_2, 600 MHz)

2A	**2B**	Assignment
7.53(d)	7.69(d)	C_6H_2
6.55(d)	a	C_6H_2
6.28(s)	a	C_5H
3.2–2.4(m)	a	C_6H_8, THF, α-CH$_3$
2.2–1.5(m)	a	C_6H_8, THF
0.65(s)	0.83(s)	$(CH_3)_2$Si
	0.80(s)	$(CH_3)_2$Si
1.30(m)		heptane
0.88(m)		heptane

[a] Presumably underneath the corresponding signals of **2A**.

from the $Mg(THF)_2$ ligand plane; this reduces the repulsion which the C_6-rings of the indenyl ligands would suffer by the THF ligands in a bis-η^5-coordinated racemo isomer.

In the bis-cyclopentadienyl complex **3**, where both C_5-ring ligands are η^5-coordinated to the Mg center, the preference for the meso configuration appears to derive from increased repulsions which both *t*-butyl substituents of the racemo isomer would incur, either from one THF ligand in a centrally located coordination site or—even more so—from two THF ligands coordinated to both lateral coordination sites.

In complex **4**, however, the η^1-coordination of one of the cyclopentadienyl rings, caused by the short Me_2Si-bridge, places the *t*-butyl substituent attached to this C_5 ring in a position quite remote from all other parts of the complex molecule (Fig. 3). This raises the question whether intramolecular interactions of the type discussed above still determine the meso configuration of this complex, or whether it derives from crystal packing effects. In order to clarify this question, also with regard to the complexes **1–3**, we have tried to determine the structures of these magnesocene complexes in solution by ^{1}H NMR methods.

2.2. ^{1}H NMR spectra and structural dynamics in solution

For the C_2H_4-bridged bis-indenyl complex **1**, $(C_2H_4)(\text{ind})_2Mg(THF)_2$, we find, in CD_2Cl_2 and C_6D_6 solutions, ^{1}H NMR spectra (Fig. 4) which indicate the presence of one dominant and one minor species with an intensity ratio of ca. 20:1 (Table 2). For the dominant species **1A**, a racemic configuration is documented by a strong NOE interaction of the α-proton of each C_5 ring (at C(5) and C(10)) with the proton in position 7 of the indenyl C_6 ring on the opposite side of the complex molecule (at C(15) and C(11)), similar to that described by Piemontesi et al. [25] for the racemic isomer of $C_2H_4(\text{ind})_2ZrCl_2$. The C_2-symmetrical appearance of the ^{1}H NMR spectrum of species **1A** indicates that the two types of η^3-coordination observed in its crystal structure (Fig. 1) are rapidly interchanging in solution.

Upon warming these solutions to 25°C, only the THF signals are observed to coalesce; in all other regards, the ^{1}H NMR spectra remain without significant change. This indicates that species **1A** and **1B** do not undergo rapid interconversion at room temperature. Significant exchange of the two species is indicated, however, by fairly strong ROESY cross signals for all corresponding proton positions.

Table 4
^{1}H NMR shifts for complex **3** (in ppm, 25°C, 600 MHz)

3A[a]	**3B**[a]	**3B**[c]	**3C**[a]	**3C**[c]	**3A**[b]	**3B**[b]	Assignment
5.84(t^p)	6.00(t^p)	6.03(t^p)	d	5.57(s)	5.96(t^p)	6.14(t^p)	C_5H_3
5.53(t^p)	5.44(t^p)	5.45(t^p)	5.28(t^p)	5.30(s)	5.56(t^p)	5.52(t^p)	C_5H_3
5.33(t^p)	4.88(t^p)	5.01(t^p)	5.11(t^p)	5.13(s)	5.47(t^p)	5.25(t^p)	C_5H_3
1.45(s)	e	1.49(s)	1.37(t^p)	1.37(s)	1.54(s)	1.59(s)	$(CH_3)_4C_2$
1.33(s)	1.27(s)	1.28(s)			1.40(s)	1.20(s)	$(CH_3)_4C_2$
1.10(s)	1.12(s)	1.11(s)	1.05(s)	1.06(s)	1.16(s)	1.14(s)	$(CH_3)_3C$

[a] In D_8-THF.
[b] In CD_2Cl_2.
[c] In D_8-THF, 50°C.
[d] Underneath signal at 5.53 ppm.
[e] Underneath signal at 1.45 ppm.

To probe the nature of this exchange process, we have studied CD_2Cl_2 solutions of complex **1**, to which small increments of THF were added. Additions of increasing amounts (1–3 equivalents) of THF cause a broadening, first of the signals of the minor species **1B**, at higher THF concentrations also of those of species **1A**. At the same time, the THF signal at 3.26 ppm is shifted to 3.47 ppm. Apparently, the interconversion of **1A** and **1B** involves the coordination of an additional THF molecule. One of these species must thus differ from the structure represented in Fig. 1 by loss or addition of a THF ligand molecule, probably accompanied by a change of hapticity in one or both of the C_5-ring ligands. Our data do not allow us to assign numbers of coordinated THF molecules for each of the

two species involved, however. While the absence of detectable cross-signals of the type discussed above for **1A** would indicate that species **1B** might represent a meso-configurated isomer, the intensity of all signals of species **1B** is so low that these cross-signals might escape detection.

For complex **2**, $(Me_2Si(2\text{-Me-thbzind})_2Mg(THF)_2$, we observe in CD_2Cl_2 solution again a major species **2A** and a minor species **2B** (Table 3). The latter has a signal intensity of ca. 24% of the major species. Species **2A** clearly represents the racemic isomer, as documented by the homotopicity of the methyl groups at the silyl bridge, for which only one ^{1}H NMR signal is observed at 0.65 ppm. The minor species **2B** appears to be the meso isomer of complex **2**, since two singlets of
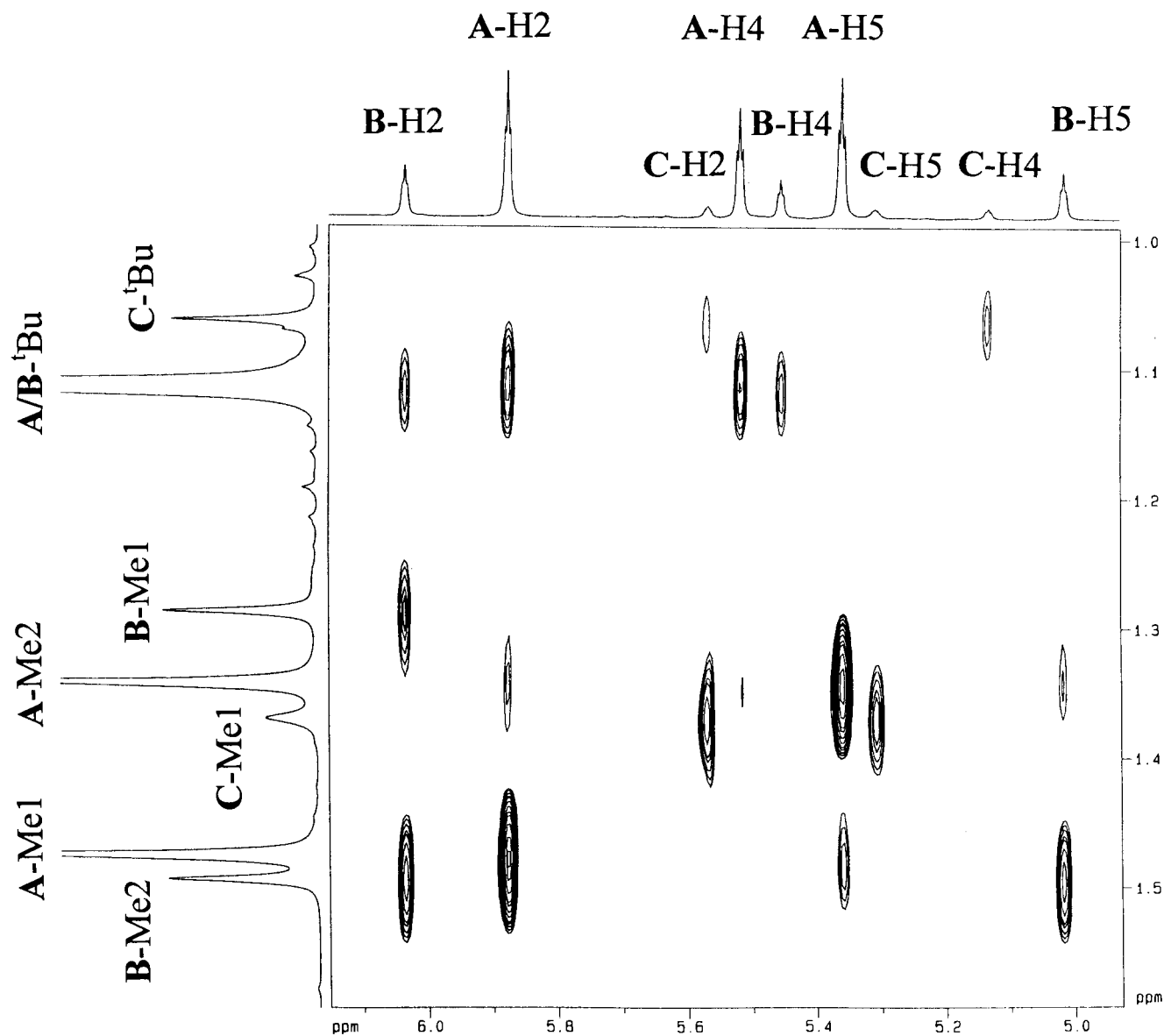

Fig. 5. ROESY spectrum of complex **3** in D_8-THF solution (50°C, 600 MHz). For species **3A** and **3B**, the H2 and H5 protons give rise to contact cross peaks with different sets of CH_3 groups at the ethano bridge.

equal intensity are observed at 0.80 and 0.83 ppm for its Me_2Si bridge. These signals give rise to strong exchange signals with the Me_2Si signal of the racemo isomer at 0.65 ppm. Apparently, the rac–meso interchange occurs at a substantial rate for complex **2**.

The tetramethylethano-bridged complex **3**, $Me_4C_2(3\text{-}{}^tBu\text{-}C_5H_3)_2Mg(THF)$, shows in its ^1H NMR spectra in CD_2Cl_2 solution again the presence of a dominant species **3A** and a minor species **3B**. The minor species **3B**, which is present in ca. 10% of species **3A**, appears to differ from species **3A** by addition of a THF molecule: Its intensity increases to ca. 16% of the main species when measured in the presence of 3 equivalents of D_8-THF and to ca. 40% in pure D_8-THF. In these D_8-THF solutions, a third species, **3C**, becomes apparent with an abundance of ca. 10% of species **3A** (Table 4). All three species give rise to strong ROESY exchange signals with each other.

Evidence with regard to the structures of these species is derived from the NOE cross peaks in their ROESY spectra (Fig. 5). For species **3A**, the α-protons in position 2 of the C_5 rings have their main NOE cross

signal with one set of CH_3 groups of the $(CH_3)_4C_2$ bridge (and with the *t*-butyl groups), while the protons in position 5 have a cross signal with the other set of bridge-CH_3 groups. Such an interaction pattern is to be expected for the meso form found for crystalline complex **3**: This geometry places the protons in position 2 (H2) in close contact, with $d(H–Me) < 300$ pm, to the bridge-methyl groups labelled Me(1), which are equivalent in the time-averaged spectra, while the protons in position 5 (H5) are close to the set of methyl groups labelled Me(2) (Fig. 6). Weak cross peaks of the 2-positioned protons with Me(2) and of the 5-positioned protons with Me(1) are in accord with cross-distances of $d(H–Me) \approx 3$–400 pm. For a racemic species, on the other hand, NOE cross peaks with the same set of bridge-CH_3 groups are to be expected for both sets of α-protons: In the *t*-butyl-forward conformation, the α-protons of type H2 as well as those of type H5 would be in close contact with the Me2 set of bridge-CH_3 groups, in the *t*-butyl-backward conformer, both H2 and H5 would have their closest contacts with the Me1 set. The mutually exclusive cross-signals observed for species
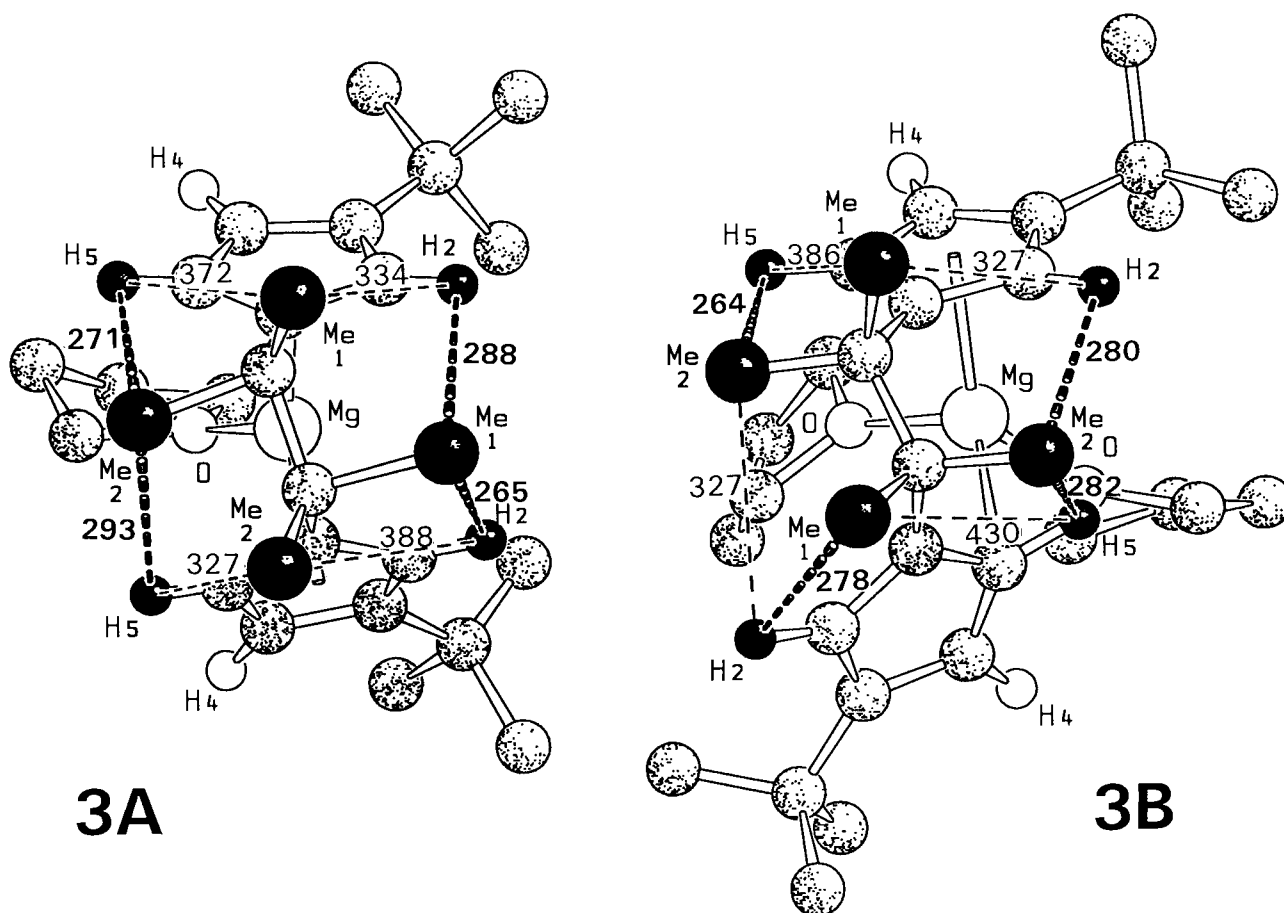

3A

3B

Fig. 6. Molecular models of the meso-configurated species **3A** (left, taken from the crystal structure) and of the rac-configurated, η^1,η^5-coordinated species **3B** (right, modelled after the crystal structures found for complexes **3** and **4**, see text); distances between H2 and H5 protons and the Me1 and Me2 sets of bridge-CH_3 groups are indicated by dashed lines (SCHAKAL graphics).

3A (Fig. 5) can thus be regarded as clear evidence that species **3A** represents the meso isomer predominating also in the crystalline state (Fig. 3).

For species **3B** and **3C**, however, both α-protons have their main contact peaks with the same set of bridge-CH_3 groups (Fig. 5). As discussed above, this phenomenon is indicative of a racemic configuration of these species. The coordination of an extra THF molecule, which is implied by the intensity increase of these species in the presence of THF, is likely to decrease the hapticity of one (or both) of the ring ligands. We have therefore constructed molecular models of a bis-THF adduct of complex **3** with one η^1-coordinated and one η^5-coordinated C_5 ring. This was done by fixing the equilibrium Mg–O distances for the THF ligands and the Mg–C distance of the η^1-coordinated C_5 ring to the respective values found for complex **4**, while keeping the Mg–C distances of the η^5-coordinated C_5 ring at the values found for crystalline complex **3** (Fig. 6).

As discussed above for racemic complexes with bis-η^5-coordination, η^1/η^5-coordinated species with pre-rac configuration (i.e., with the t-butyl groups on opposite sides of the C(ipso)–Mg–C(ipso) plane) are found to have their H2 and H5 protons in closest contact with the same set of bridge-CH_3 groups. That conformation at the C_2 bridge, in particular, which puts both t-butyl groups in their 'backward' position (Fig. 6), is found to reproduce exactly the contact pattern observed for species **3B** (Fig. 5): while both the H2 and H5 protons are in closest contact with the Me2 set of bridge-CH_3 groups, one of the H2 protons is also in reasonably close contact to Me1. As this pattern cannot arise for any meso-configured isomer of complex **3**, we can assign rac-type configurations to species **3B** and **3C**. The symmetrical ^{1}H NMR spectra observed for both of these species indicate a rapid interchange between η^1-coordinated and η^5-coordinated C_5 rings. A similarly fast η^1/η^5-interchange has recently been observed for complexes of the type $CMe_2(\eta^1$-$C_5H_4)(\eta^5$-$C_5H_4)$(Nb, Ta)(NAr)(NMe$_2$) [26]. The difference between species **3B** and **3C** might arise from the number of their THF ligands: Species **3B** is seen already in the presence of a few equivalents of THF in CD_2Cl_2, species **3C** only in pure D_8-THF. Species **3C** is thus likely to contain a third THF ligand; an η^1-coordination of both C_5 rings in species **3C**, caused by this extra ligand, would be consistent with its NOE pattern.

For the Me_2Si-bridged magnesocene **4**, $Me_2Si(3$-^tBu-$C_5H_3)_2Mg(THF)_2$, finally, we observe ^{1}H NMR spectra in CD_2Cl_2 or C_6D_6 solutions, which are—with more than ten t-butyl signals and about the same number of $SiMe_2$ signals—far too complicated for any straightforward interpretation. In D_8-THF solution, the ^{1}H NMR spectra are somewhat simplified, but even here, we observe at least four species with abundancies

which depend on total magnesocene concentrations. This and the unusually broad Me_2Si signals of some of these species raises the possibility that these solutions might contain oligomers of complex **4**, in which the alternative between a highly strained geometry and an unfavourable η^1 coordination is avoided by the coordination of Mg centers to C_5 rings from two different Me_2Si-bridged ligand units. That polynuclear metallocene complexes with many metal centers are easily formed with Me_2Si-bridged bis-cyclopentadienyl ligands has recently been shown for complexes of composition $((Me_2Si)_2(C_5H_3)_2Fe)_n$ [27].

3. Conclusions

A preference for the racemic isomer similar to that found in the solid state is indicated for complexes **1** and **2** by the ^{1}H NMR data obtained in CD_2Cl_2 solution. For complex **3**, the meso configuration of the crystalline complex appears to predominate also in solution. For these complexes, the intramolecular interactions which favor a particular diastereomer thus appear to be the same in the solid state as in solution. In solution, however, the other diastereomer appears as a minor species. For complexes **1** and **2**, meso isomer fractions of ca. 5 and 20% indicate free-energy differences of ca. 4–6 kJ/mol between rac and meso diastereomers. For complex **3**, the free-energy difference between the major and the minor isomer is of similar magnitude; here, addition of THF appears to stabilize the racemic isomer. For complex **4**, finally, our data do not afford any conclusions with regard to the relative abundance of racemic and meso isomers in solution.

From the intensity of their ROESY exchange signals we can estimate that meso and rac diastereomers interconvert with half-lives in the order of a few seconds. With regard to the mechanisms of these meso-rac interconversions, it remains to be clarified whether the Mg center moves from one enantioface of the C_X ligand fragment to the other by way of a bimolecular S_E2-type exchange reaction or via a de-coordinated η^0-type species [18], possibly stabilized by extra THF ligands. Fast equilibria involving loss or uptake of THF ligands, observed especially in solutions of complexes **1** and **3**, might intervene in the interconversion of rac and meso diastereomers: the facile interconversion observed for species **3A**, **3B** and **3C**, e.g., might be due to the circumstance that only one THF molecule fits into the tight crevice of **3A** and that additional THF ligands coordinated to the Mg center in **3B** and **3C** are likely to repel the bulky C_5-ring substituents to such a degree that de-coordination of one C_5-ring is facilitated.

We are presently studying how the changing hapticities, diastereomer preferences and interconversion rates of chiral ansa-magnesocenes of the type described above

intervene in the utilization of these compounds as synthons for other chiral ansa-metallocene complexes.

4. Experimental

4.1. General information

All manipulations were performed on an argon/vacuum manifold or in a glove-box under nitrogen atmosphere. Solvents were dried over sodium/benzophenone, degassed under reduced pressure and stored under argon. $C_2H_4(indH)_2$ [28], $Me_2Si(3-3'-(2-Me-tetrahydrobenz[e]ind)_2$ [1], $C_2(CH_3)_4(3-t-BuC_5H_4)_2$ [29] and $Me_2Si(3-t-Bu-C_5H_4)_2$ [24] were prepared according to previous reports. $(n,s-Bu)_2Mg$ (1.0 M in heptane) was obtained from Aldrich. ^{1}H NMR spectra were recorded on Bruker AC 250, Bruker WM 250 or Bruker DRX 600 spectrometers.

4.2. $C_2H_4(ind)_2Mg(THF)_2$ (1)

To a solution of $C_2H_4(indH)_2$ (1.49 g, 5.77 mmol) in 150 ml of heptane added a 1.0 M solution of dibutylmagnesium (6.3 mmol, 6.3 ml) in heptane. The mixture was heated to reflux for 5 h; during this period a light yellow product precipitated. Excess gas pressure of butane was allowed to escape via a bubbler. The solution was cooled to $-30°C$, decanted and the precipitate washed with small amounts of heptane. Drying in vacuo yields 1.46 g (90%) of a light yellow powder (presumably THF-free complex 1), which was dissolved in a small amount of THF and covered with a layer of hexane. Violetish, needlelike crystals, which separated after several days at room temperature, were collected by decantation and dried in vacuo to give 0.98 g (40% theoretical yield) of complex 1. Further concentration of the mother liquor and cooling to $-30°C$ yielded an additional crop of 0.88 g (36%) of 1. ^{1}H NMR in CD_2Cl_2 and C_6D_6 solution see Table 2. Anal. Found C, 78.53; H, 7.70. $C_{28}H_{32}MgO_2$ (424.87) Calc.: C, 79.15; H, 7.59%.

4.3. $Me_2Si(2-Me-tetrahydrobenz[e]inden-3-yl)_2Mg(THF)_2(C_7H_{16})_{0.5}$ (2)

To a solution of 1.00 g of $Me_2Si(2-Me-tetrahydrobenz[e]indenene)_2$ (2.35 mmol) in 100 ml heptane was added 2.5 ml of a 1.0 M solution of dibutylmagnesium (2.5 mmol) in heptane. The mixture was heated to reflux for 6 h. After cooling to room temperature, 0.4 ml of THF (4.9 mmol) was added. Yellow–green needles, formed after several days, were collected by decantation, washed with small amounts of heptane and dried in vacuo to give 0.35 g crystals of complex 4,

which contain half a molecule of heptane per magnesocene (23% theoretical yield). Further concentration and cooling to $-30°C$ gave an additional 0.2 g (14%) of 2. ^{1}H NMR in CD_2Cl_2 see Table 3. Anal. Found C, 78.04; H, 9.12. $C_{41.5}H_{58}MgO_2Si$ (641.30) Calcd.: C, 77.72; H, 9.11%.

4.4. $(CH_3)_4C_2(3-{}^tBu-C_5H_3)Mg(THF)$ (3)

To a solution of 6.78 g of $(CH_3)_4C_2(3-{}^tBu-C_5H_4)_2$ (20.76 mmol) in 200 ml heptane was added 23 ml of a 1.0 M solution of dibutylmagnesium (23 mmol) in heptane. The solution was heated to reflux for 5 h and excess gas was allowed to escape via a bubbler. The slightly yellow solution was treated with 4 ml of THF (49 mmol), stirred 1 h at room temperature, concentrated to a quarter of its volume and cooled to $-30°C$. After several days, colorless crystal had separated, which were collected by decantation, washed with small amounts of heptane and dried in vacuo to give 6.83 g $C_2(CH_3)_4(3-t-Bu-C_5H_3)_2Mg(THF)$ (3, 78% theoretical yield). Further concentration and cooling to $-30°C$ gave additional 0.35 g (4%) of 3. ^{1}H NMR in CD_2Cl_2 solution see Table 4. Anal. Found: C, 79.5; H, 10.19. $C_{28}H_{44}MgO$ (420.96) Calc.: C, 79.89; H, 10.53%.

4.5. $Me_2Si(3-{}^tBu-C_5H_3)_2Mg(THF)_2$ (4)

To a solution of 5.37 g of $Me_2Si(3-{}^tBu-C_5H_4)_2$ (17.86 mmol) in 200 ml of heptane 19.65 ml of a 1 M solution (19.65 mmol) of dibutylmagnesium in heptane was added. The mixture was heated to reflux for 5 h, allowing excess gas pressure to escape via a bubbler. The clear solution was concentrated under reduced pressure to approximately one third of its volume. Addition of 3 ml of THF (36.86 mmol) at room temperature and cooling to $-30°C$ resulted, after several days, in the deposition of colorless crystals which were collected by decantation, washed with small amounts of heptane and dried in vacuo to yield 5.1 g of complex 4 (61% theoretical yield). Further concentration of the mother liquor and cooling gave additional 2.0 g (24%) of complex 4. ^{1}H NMR in CD_2Cl_2 and D[8]-THF see Table 5. Anal. Found: C, 71.68; H, 9.80. $C_{28}H_{46}MgO_2Si$ (467.06) Calc.: C, 72.0; H, 9.92%.

Table 5
^{1}H NMR shifts for complex 4 (in ppm, 25°C, D_8-THF, 5.2 mg/0.5 ml, 600 MHz)

4A	4B	4C	4D	Assignment
6.14(s)	5.68(s)	6.35(t^p);	6.33(t^p)	C_5H_3
6.00(t^p)	5.64(s)	6.23(t^p);	6.20(t^p)	C_5H_3
5.69(t^p)	5.57(s)	5.94(m)	5.94(m)	C_5H_3
1.16(s)	1.09(s)	1.22(s) or 1.20(s)	1.22(s) or 1.20(s)	$(CH_3)_3C$
		1.20(s) or 1.20(s)	1.20(s) or 1.20(s)	$(CH_3)_3C$
0.37(b)	0.42(s)	0.44(s);	0.41(s); 0.35(s)	$(CH_3)_2Si$

Table 6
Crystallographic and experimental data for complexes **1**–**4**[a]

Complex	1	2	3	4
Formula	$C_{28}H_{32}MgO_2$	$C_{38}H_{50}MgO_2Si \cdot (C_7H_{16})_{0.5}$	$C_{28}H_{44}MgO$	$C_{28}H_{46}MgO_2Si$
Color, habit	red rhombohedron	colorless plates	colorless plates	colorless rhombohedron
Diffractometer	Siemens P4	Enraf Nonius CAD 4	Siemens P4	Siemens P3R3
Space group	$P2/n$	$P2(1)/n$	$Pna2(1)$	$P2(1)/n$
a (Å)	8.883(2)	14.473(5)	11.306(4)	14.97(1)
b (Å)	29.120(6)	13.108(2)	20.038(5)	14.011(9)
c (Å)	17.168(3)	16.673(7)	11.519(4)	15.26(1)
β (deg)	94.98(1)	99.67(2)		114.74(5)
Volume (Å^3)	4424.1(16)	7399.8(39)	2609.5(15)	2908(4)
Z	8	8	4	4
d(calc.)/(g cm^{-3})	1.276	1.151	1.071	1.067
Absorption coefficient μ mm^{-1}	0.103	0.114	0.084	0.117
Temperature (K)	167	133	213	293
Weighting scheme (A,B)	0.0572, 2.9373[b]	0.1149, 9.191[b]	0.138, 2.387[b]	0.00004[c]
2θ range/deg	3.7 to 55.0	4.1 to 50	4.1 to 44.0	4.0 to 48.0
Scan speed/(deg min^{-1})	4.0 to 60.0	2.0 to 16.5	3.0 to 30.0	1.5 to 14.650
Scan range/deg	1.7	1.0	0.9	1.6
Scan type	Adaptive ω	$\omega/2\theta$	$\omega/2\theta$	Wyckoff
Reflection collected	10 496	13 521	3005	2796
Independent reflections	10 147	12 974	3005	2520
Observed reflections	6367 [$I > 2\sigma(I)$]	6128 [$I > 2\sigma(I)$]	1709 [$I > 2\sigma(I)$]	2012 [$F > 4.5\sigma(F)$]
Solution	Direct	Direct	Direct	Direct
Refinement	Shelx 93[d]	Shelx 93[d]	Shelx 93[d]	Shelx 86[d]
Number of parameters	555	819	271	315
R_f	5.84%	9.28%	9.98%	11.05
R_w	13%[e]	21.7%[e]	23.6%[e]	11.8[f]
Goodness of fit	1.044	1.049	1.053	7.5
Residual density/(e Å^{-3})	0.38/ − 0.32	0.61/ − 0.40	0.34/ − 0.25	0.69/ − 0.47

[a] Mo Kα radiation, 71.073 pm, graphite monochromator.
[b] $w^{-1} = \sigma^2(F_o^2) + (A \cdot P)^2 + B \cdot P$, where $P = (F_o^2 + 2F_c^2)/3$.
[c] $w^{-1} = \sigma^2(F^2) + AF^2$.
[d] G. Sheldrick, University of Göttingen 1986 and 1993.
[e] Based on F^2.
[f] based on F.

4.6. Diffractometric structure determinations

Crystallographic and experimental data pertaining to the structure determinations of complexes **1**–**4** are summarized in Table 6, selected bond distances and angles in Table 1. Additional crystallographic data can be obtained from Fachinformationszentrum Karlsruhe, D-76344 Eggenstein-Leopoldshafen 2, upon quotation of the depository numbers CSD-407844 to CSD-407877, the names of the authors and the journal reference for this article.

Acknowledgements

References

[1] N. Schneider, M.E. Huttenloch, U. Stehling, R. Kirsten, F. Schaper, H.H. Brintzinger, Organometallics 16 (1997) 3413.
[2] R.A. Andersen, J.M. Boncella, C.J. Burns, R. Blom, A. Haaland, H.V. Volden, J. Organomet. Chem. 312 (1986) C49.
[3] R.A. Andersen, R. Blom, C.J. Burns, H.V. Volden, J. Chem. Soc., Chem. Commun. (1987) 768.
[4] R. Blom, K. Faegri Jr., H.V. Volden, Organometallics 9 (1990) 372.
[5] R.A. Williams, T.P. Hanusa, J.C. Huffmann, J. Chem. Soc., Chem. Commun. (1988) 1045.
[6] R.A. Williams, T.P. Hanusa, J.C. Huffmann, Organometallics 9 (1990) 1128.
[7] J.S. Overby, T.P. Hanusa, Organometallics 15 (1996) 2205.
[8] M. Rieckhoff, U. Pieper, D. Stalke, F.T. Edelmann, Angew. Chem., Int. Ed. Engl. 32 (1993) 1079.

[9] R. Littger, N. Metzler, H. Nöth, M. Wagner, Chem. Ber. 127 (1994) 1901.

[10] S. Harder, M. Lutz, A.W.G. Straub, Organometallics 16 (1997) 107.

[11] W. Bünder, E. Weiss, J. Organomet. Chem. 92 (1975) 1.

[12] M.G. Gardiner, C.L. Raston, C.L. Kennard, Organometallics 10 (1991) 3680.

[13] R.A. Andersen, R. Blom, J.M. Boncella, C.J. Burns, H.V. Volden, Acta Chem. Scand. A41 (1987) 24.

[14] P. Burger, Chimia 50 (1996) 329.

[15] A.W. Duff, P.B. Hitchcock, M.F. Lappert, R.G. Taylor, J.A. Segal, J. Organomet. Chem. 293 (1985) 271.

[16] J.J. Eisch, R. Sanchez, J. Organomet. Chem. 296 (1985) C27.

[17] R. Lisowsky, Europ. Pat. Appl. 94112299.6 (1994).

[18] J.M. O'Connor, C.P. Casey, Chem. Rev. 87 (1987) 307.

[19] G.M. Diamond, M.L. Green, P. Mountford, N.A. Popham, A.N. Chernega, J. Chem. Soc., Chem. Commun. (1994) 103.

[20] M. Bochmann, S. Lancaster, M.B. Hursthouse, M. Mazid, Organometallics 12 (1993) 4718.

[21] O. Koch, F. Edelmann, B. Lubke, U. Behrens, Chem. Ber. 115 (1982) 3049.

[22] F. Schaper, M. Rentzsch, M.H. Prosenc, U. Rief, K. Schmidt, H.H. Brintzinger, J. Organomet. Chem. 534 (1997) 67.

[23] A. Schäfer, E. Karl, L. Zsolnai, G. Huttner, H.H. Brintzinger, J. Organomet. Chem. 328 (1987) 87.

[24] H. Wiesenfeldt, A. Reinmuth, E. Barsties, K. Evertz, H.H. Brintzinger, J. Organomet. Chem. 369 (1989) 359.

[25] F. Piemontesi, I. Camurati, L. Resconi, D. Balboni, A. Sironi, M. Moret, R. Zeigler, N. Piccolrovazzi, Organometallics 14 (1995) 1256.

[26] W.A. Herrmann, W. Baratta, E. Herdtweck, Angew. Chem., Int. Ed. Engl. 35 (1996) 1951.

[27] B. Grossmann, J. Heinze, E. Herdtweck, F.H. Köhler, H. Nöth, H. Schwenk, M. Spiegler, W. Wachter, B. Weber, Angew. Chem., Int. Ed. Engl. 36 (1997) 387.

[28] F.R.W.P. Wild, L. Zsolnai, G. Huttner, H.H. Brintzinger, J. Organomet. Chem. 232 (1982) 233.

[29] S. Gutmann, P. Burger, H.U. Hund, J. Hofmann, H.H. Brintzinger, J. Organomet. Chem. 369 (1989) 343.